Resonant-Raman intensities and transition energies of the E_{11} transition in carbon nanotubes

H. Telg,[1,*] J. Maultzsch,[1] S. Reich,[2] and C. Thomsen[1]
[1]*Institut für Festkörperphysik, Technische Universität Berlin, Hardenbergstrasse 36, 10623 Berlin, Germany*
[2]*Department of Materials Science and Engineering, Massachusetts Institute of Technology, 77 Massachusetts Avenue, Cambridge, Massachusetts 02139-4307, USA*

(Received 12 May 2006; revised manuscript received 25 July 2006; published 27 September 2006)

We observed the lowest optical transitions (E_{11}^S) in separated carbon nanotubes by resonant Raman spectroscopy. Radial breathing mode spectra were collected varying the excitation energy in the near-infrared from 1.15 to 1.48 eV. From resonance profiles we obtained the E_{11}^S energies of 11 nanotubes, extending the experimental Kataura plot. Strong Raman signal from tubes with $\nu=(n-m)\mathrm{mod}3=+1$ and from tubes that were absent in photoluminescence support the theory of exciton resonance. The measured Raman intensities agree well with the calculated optical absorption and electron-phonon coupling obtained with first-principles and empirical methods. A remaining factor of ~3 can be due to a higher abundance of armchairlike tubes or differences of the absorption and vibrational coupling between correlated (excitons) and uncorrelated electron-hole pairs.

DOI: 10.1103/PhysRevB.74.115415 PACS number(s): 78.67.Ch, 73.22.−f, 78.30.Na, 81.07.De

A large effort is devoted to controlling the atomic structure—the so-called chiral index[1] —of carbon nanotubes either during the growth process[2,3] or by sorting the tubes by subsequent chemical treatment[4] and electrophoresis.[5] In spite of constant progress, most nanotube samples contain a large variety of different chiral indices (n,m). There is a tremendous need for a quick and nondestructive characterization of the chiral index and relative (n,m) abundances. Common techniques to probe the chiral indices in a nanotube ensemble are photoluminescence excitation (PLE)[6] and resonance Raman spectroscopy (RRS).[7,8] While PLE measurements require a smaller experimental effort, RRS has the advantage of a more straightforward sample preparation and the virtue that metallic nanotubes can be observed. Both methods have led to so-called experimental Kataura plots, which can be used to identify uniquely the chiral index of a nanotube.

Recently, the results of PLE and RRS experiments were used to determine the relative abundance of different chiral indices (n,m) in nanotube samples by comparing the amplitude of the respective signal for different nanotubes.[6,9,10] Depending on the method, this led to different results and to controversial interpretations concerning the relative abundance of certain nanotubes. While zigzag tubes were not seen in PLE experiments on HiPCO tubes dissolved in SDS (sodium dodecyl sulfate) and therefore claimed to be absent,[6] they were observed in RRS measurements of the same samples.[7,8] Another difference is that in PLE the strongest signal was observed from nanotubes with large chiral angles (close to armchair), with a decreasing intensity towards smaller angles.[6] RRS experiments, in contrast, showed a maximum intensity for tubes with chiral angles of $\approx 15°$.[7]

The resonant Raman intensity depends on the nanotube family $\nu=(n-m)\mathrm{mod}3=\pm 1$.[11] For excitation into the E_{22}^S bands in tubes with similar diameter, the resonance and luminescence maxima were much weaker for the $\nu=+1$ family than for the $\nu=-1$ family. This mod3 family dependence of the Raman intensity was predicted theoretically and originates from a mod3 dependence of the electron-phonon matrix element.[12,13] Furthermore, nanotubes with small chiral angles and $\nu=+1$ were not observed in PLE. An explanation of this effect, which further complicates the determination of abundances, was given by Reich *et al.*[14] They introduced an exciton-exciton resonance which can occur when exciting the second (or higher) optical transition E_{22}^S in nanotubes.[15] For experimental reasons, in most published RRS experiments the second or higher optical transitions are excited. Therefore the signal intensity in these experiments is affected by the exciton resonance. In contrast, Raman scattering in resonance with the *first* optical transition E_{11}^S cannot be affected by exciton resonances and therefore might be the appropriate technique to determine abundances of (n,m).

In this paper, we report the energies of the first optical transition E_{11}^S of 11 semiconducting single-walled carbon nanotubes by resonant Raman spectroscopy. We extend the experimental Kataura plot into the infrared range of transition energies. We observe several nanotubes with small chiral angle and $\nu=+1$ family that were not detected in luminescence. The intensity difference between tubes with $\nu=+1$ and those with $\nu=-1$ is much smaller than for E_{22}^S transitions. Our results confirm the systematic family-index dependence of transition strength and electron-phonon coupling in nanotubes and support the theory of exciton resonance in carbon nanotubes.

We performed resonance Raman spectroscopy on single-walled carbon nanotubes produced by the HiPCO method. The nanotubes were ultrasonically dispersed in D_2O and stabilized in sodium dodecyl sulfate (SDS) micelles.[16,17] A TiSa-laser was used to vary the excitation energy between 1.148 and 1.476 eV. We collected the low-energy Raman spectra using a triple monochromator and an InGaAs reticon. Spectra were normalized to the integration time t, laser power P_l, system response $R(\omega_s)$, frequency of the scattered light ω_s to the power of four, phonon energy ω_{ph}, and Bose-Einstein occupation number N. The thus corrected intensity of a given Raman peak in resonance is proportional to the square of the Raman susceptibility:[18]

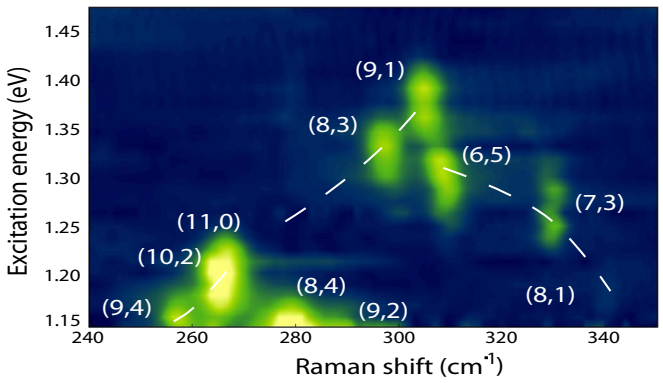

FIG. 1. (Color online) Contour plot of the normalized Raman spectra as a function of excitation energy. See Eq. (1) for the normalization.

$$|\chi|^2 = c\frac{I(\omega_s)\omega_{ph}}{R(\omega_s)P_l t\omega_s^4(N+1)}, \tag{1}$$

where $I(\omega_s)$ is the detected signal intensity and c includes the remaining factors.

Figure 1 shows a contour plot of the Raman spectra as a function of excitation energy. It covers the low-energy region of the nanotube Raman spectrum where the radial breathing mode (RBM) is observed. The RBM frequency ω_{RBM} depends inversely on the diameter of the nanotube and is only seen when the excitation energy is close to the transition energy of the nanotube. The separation of nanotubes with different (n,m) in the observed region of diameter is large enough that each bright spot in Fig. 1 corresponds to a nanotube with different chiral index (n,m). For each RBM peak we analyzed the resonance profile by fitting the excitation-energy dependence to the first-order Raman cross section:[18,19]

$$I(E_l) = \left(\frac{\mathcal{M}c'}{\hbar\omega_{\mathrm{RBM}}}\right)^2 \left| \frac{1}{(E_l - E_{ii} - i\gamma/2)} - \frac{1}{(E_l - \hbar\omega_{\mathrm{RBM}} - E_{ii} - i\gamma/2)} \right|^2, \tag{2}$$

where E_l is the laser energy, E_{ii} the energy of the allowed optical transition, and γ the lifetime broadening of the intermediate electronic state. $\mathcal{M}$ contains the matrix elements and c' includes all remaining factors. The first term in Eq. (2) corresponds to incoming and the second term to outgoing resonance. Best fits of the parameter $E_{ii}=E_{11}^S$ are listed in Table I. The chiral index related to each RBM in Fig. 1 was found from the assigned RBM frequencies from Ref. 7 and by comparing the E_{11}^S (Table I) with the Kataura plot pattern predicted from a tight-binding approximation.[7,20]

Figure 2 shows the extended experimental Kataura plot including the E_{11}^S optical transitions of 11 nanotubes (closed circles). Open symbols are data from Refs. 7 and 21 representing the E_{22}^S transitions of semiconducting (circles) and E_{11}^M of metallic (diamonds) nanotubes. In Fig. 2, the closed symbols (this work) are vertically aligned with the corresponding E_{22}^S transitions assigned previously. The branches of the Kataura plot have the same characteristic curvature,

TABLE I. Radial breathing mode frequency ω_{RBM}, energy of the first optical transition E_{11}^S, and maximum Raman intensity I_{max} of the observed nanotubes. The transition energies were obtained from fitting Eq. (2) to the resonance profiles. Values for I_{max} are in arbitrary units. They are fully corrected and therefore proportional to the square of the Raman susceptibility $|\chi|^2$ [Eq. (1)]. Accuracies of ω_{RBM}, E_{11}^S, and I_{max} are 0.5 cm^{-1}, 10 meV (30 meV when only two digits are given), and 0.3, respectively. Italicized values are lower limits of the intensities, since the maximum of the respective resonance profile was outside the range of our experimental data.

ν	(n,m)	ω_{RBM} (cm^{-1})	E_{11}^S (eV)	I_{max}
−1	(9,1)	304.5	1.362	6.0
	(8,3)	297.0	1.306	6.6
−1	(11,0)	267.0	1.191	4.9
	(10,2)	265.0	1.173	8.1
	(9,4)	256.8	1.14	*4.7*
1	(8,1)	340.0	1.161	0.4
	(7,3)	329.5	1.249	2.4
	(6,5)	309.0	1.283	5.3
1	(9,2)	289.0	1.10	*1.7*
	(8,4)	278.8	1.12	*14*
	(7,6)	264.0	1.11	*2.0*

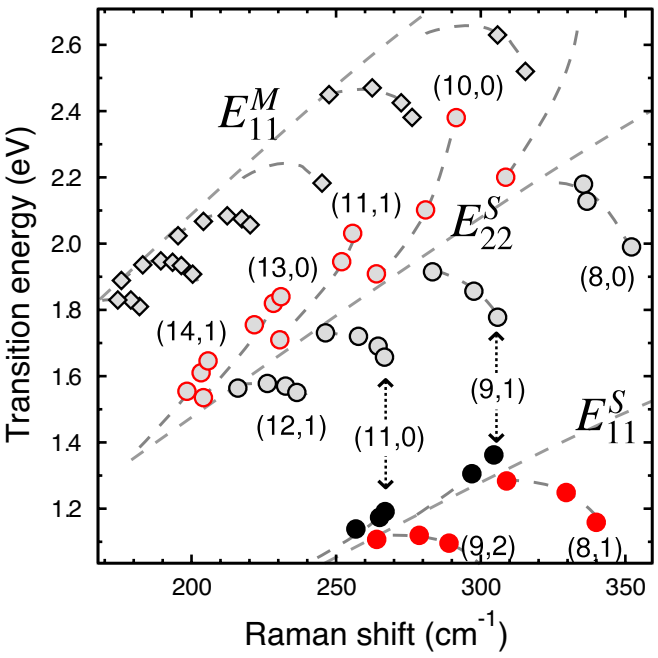

FIG. 2. (Color online) Experimental Kataura plot showing the energy of the first optical transition in metallic tubes E_{11}^M (diamonds), the first E_{11}^S (closed circles), and second E_{22}^S (open circles) optical transitions in semiconducting tubes. Semiconducting branches are labeled by the tube with the largest RBM frequency. Red (gray) circles are tubes with $\nu=+1$, black circles with $\nu=-1$. Open symbols are taken from Ref. 21.

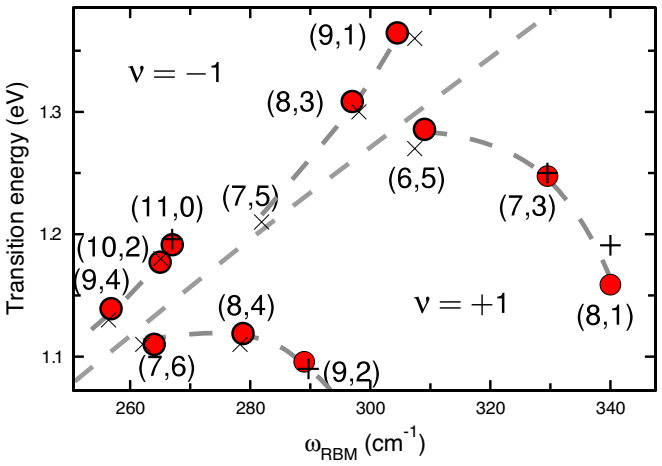

FIG. 3. (Color online) Experimental Kataura plot of the first transitions of semiconducting nanotubes E_{11}^S (lower part of Fig. 2). Results from RRS (circles) and PLE (crosses). Plus symbols are empirical data based on PLE data. (PLE and empirical data are taken from Refs. 6 and 22, respectively.)

both for the E_{11}^S and the higher-lying branches. The maximum deviation from the $1/d$ average behavior occurs for zigzaglike tubes, the minimum one for the close-to-armchair configuration. Within a branch, the neighboring chiral indices are related by $(n',m')=(n-1,m+2)$, and the nanotubes have similar physical properties.[19] The curvature of the branches is caused by the trigonal warping of the electronic bands around the K point in the graphene k-space.[11] The transitions of the two nanotube families $\nu=\pm1$ occur on opposite sides of the K point. Branches of one family are bent upwards while branches of the other family are bent downwards. Figure 2 shows that for E_{22}^S the $\nu=-1$ branches are bent downwards and those with $\nu=+1$ are bent upwards. For E_{11}^S we observe that the upward/downward curvature is reversed: branches with $\nu=-1$, such as the one labeled (11,0) or the (9,1), are bent upwards for E_{11}^S while they are bent downwards for E_{22}^S and *vice versa* in case of $\nu=+1$ branches. This result is expected since transitions of the two families are at alternating sides of the K point in graphene.

Figure 3 is an enlargement of Fig. 2 with only the E_{11}^S optical transitions from RRS (circles). The crosses reproduce the emission energies from PLE reported by Bachilo *et al.*[6] Since some tubes are not seen in PLE, we give extrapolations of PLE data for those tubes[22] (plusses). A comparison of the transition energies from Raman and luminescence shows an agreement to within ±10 meV, the accuracy of the measurements. The extrapolated data agree as well with our experimental results except for the (8,1) tube, which is predicted 30 meV higher than the experiment. The reason for this deviation is probably the very small diameter of the (8,1) tube and curvature-induced effects, which were underestimated in the empirical description of Ref. 22.

We observe several tubes that are absent in PLE spectra;[6] the (8,1), (7,3), and (9,2). Reich *et al.*[14] predicted a strong decrease of the E_{22}^S absorption strength for tubes with $E_{22}^S > 2E_{11}^S$ due to exciton-exciton resonance.[15] This relation is met by nanotubes with small chiral angles and $\nu=+1$, which

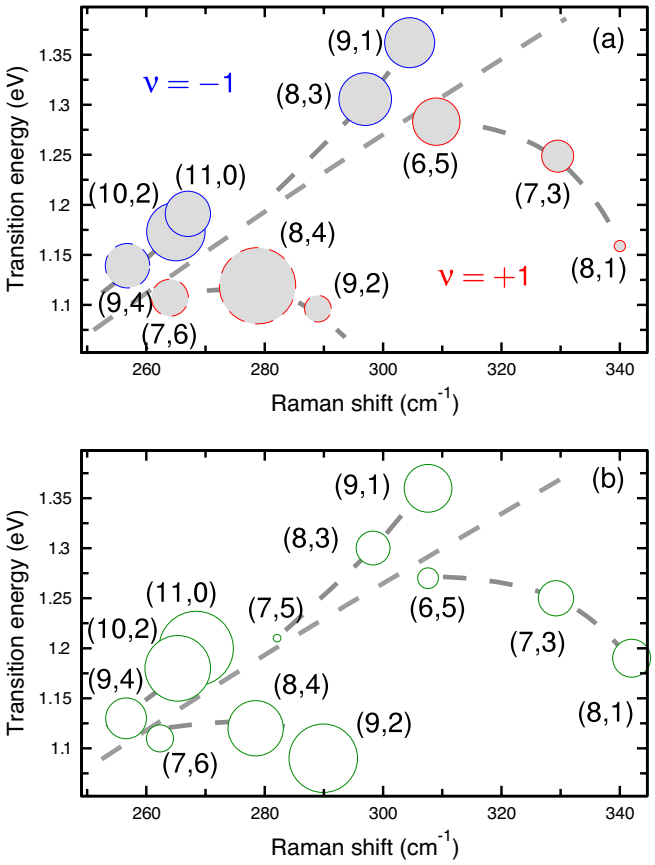

FIG. 4. (Color online) Experimental Kataura plot displaying the resonance intensity I_{max} of the Raman signal by the area of the circles. (a) Blue and red circles are nanotubes with $\nu=-1$ and $\nu=+1$, respectively. Dashed circles are tubes with resonance energies slightly outside the excitation range. For these tubes the circle areas give a lower limit of the intensities. (b) Calculated Raman intensities taken from Ref. 13 weighted by a Gaussian diameter distribution with parameters based on the (n,m) assignment of the same type of sample (Ref. 7) (average $d_0=10$ Å and standard deviation $\sigma=1.5$ Å).

is the case for the three tubes named above. In PLE, excitons are excited via E_{22}^S, and the signal of these tubes is quenched. In contrast, in resonant Raman scattering on E_{11}^S, the exciton resonance plays no role, and a strong signal of the small chiral angle $\nu=+1$ tubes is indeed observed.

The (11,0) tube, which belongs to the $\nu=-1$ family, is not observed in PLE, although it appears in the RRS measurements. The reason for the apparent absence in PLE is still unclear. It can be due to the very small energy difference between the transitions of the (11,0) and (10,2) tubes, which are difficult to resolve in PLE ($\Delta E_{11}^S \approx 20$ meV, $\Delta E_{22}^S \approx 30$ meV). In Raman measurements, the chiral index resolution is higher than in PLE; it is given by the width of the Raman peaks. We measured a full width at half maximum $(4\pm1)\text{cm}^{-1}$, therefore a difference of 2 cm^{-1} of the peak positions $\Delta\omega_{\text{RBM}}$ is required to resolve neighboring peaks. The (11,0) and the (10,2) tubes ($\Delta\omega_{\text{RBM}} \approx 2\text{cm}^{-1}$) are thus detected separately.

Figure 4 shows the Raman intensities in resonance for the tubes in Fig. 3 (see also Table I). The area of a circle is

proportional to the maximum in the square of the Raman susceptibility [Eq. (1)] of a given chiral index. In case of the (7,6), the (8,4), and the (9,2) tubes (dashed circles) only the high-energy slopes of the resonance profiles are observed. Therefore we give the maximum intensity observed in the experiments as the lower limit of the intensity.

In striking contrast to the corresponding E_{22}^S plot,[21,23] the intensities in Fig. 3 are similar for $\nu=+1$ and $\nu=-1$. This tendency can also be seen in the Raman data from Doorn *et al.*[23,24] The largest intensity in Fig. 4 is observed for the (8,4) tube. The resonance energy of this tube is probably $\approx$15 meV below our observed excitation energy range [PLE, Ref. 6, reported $E_{11}^S=1.114$ eV for the (8,4) tube]. This implies that the maximum Raman intensity of the (8,4) tube is somewhat larger than shown in Fig. 4. A clear finding of our experiment is thus that $\nu=+1$ nanotubes have an intensity equal or larger than the $\nu=-1$ nanotubes for the E_{11}^S optical transition. This is reversed for the E_{22}^S transitions of the same nanotubes, which showed a four to ten times larger intensity for the $\nu=-1$ compared to the $\nu=+1$ families.

Our results are in good agreement with predictions from *ab initio* calculations of the electron-phonon coupling[12] and tight-binding calculations[13] of the RBM Raman intensity. *Ab initio* calculations show a dependence of the electron-phonon coupling matrix element $\mathcal{M}_{\mathrm{e-ph}}$ on the nanotube family ν.[12] Machón *et al.*[12] predict this dependence to be reversed for E_{11}^S compared to E_{22}^S due to the different qualitative behavior of the $\mathcal{M}_{\mathrm{e-ph}}$ on the two sides of the K point. For example, they predicted for the E_{11}^S transition an intensity ratio of 1.8:1 between the (10,0) ($\nu=+1$) and (11,0) ($\nu=-1$) tubes. For E_{22}^S they predict the ratio for the same tubes to be reversed, 1:2.7. This agrees qualitatively with the experimental results. Experimentally, the ratio for E_{22}^S is more like 1:10,[21,23] an effect of the exciton resonance.[14] The Raman intensity depends on the absorption strength to the power of 4. The absorption quenching due to exciton resonance for E_{22}^S can thus explain the very small E_{22}^S Raman intensities of tubes with small chiral angles and $\nu=+1$. We expect that this theory will be further supported by comparing the Raman intensities of E_{11}^S and E_{22}^S for the same tube.

Let us now address the relative (n,m) intensities in nanotube ensembles. Figure 4(b) shows the Raman intensities of the nanotubes in resonance as calculated by Popov *et al.*[13] for a Gaussian diameter distribution in the range of interest here. The calculations include electron-phonon coupling and absorption while excitonic effects were ignored. Experiment [Fig. 4(a)] and theory [Fig. 4(b)] show good general and even quantitative agreement; in particular the intensities of tubes with $\nu=-1$ (upper branches) match well. Note, e.g., the (7,5) nanotube, for which the calculation predicts a very small intensity: indeed, this tube is not observed in experiment. There are, however, subtle differences between the single-particle theory and experiment. Experimentally, the last tubes in the $\nu=+1$ branches [(9,1) and (11,0)] have a weaker or similar intensity compared to the second to the last. This result was also observed in RRS on the E_{22}^S optical transitions[7] and is in contrast to the increasing intensity predicted from tight-binding for decreasing chiral angle within a branch in Fig. 4(b). The differences are larger for the armchair like nanotubes of the lower branches [$\nu=+1$, (6,5) and (8,4)]. The predicted intensities of these tubes are much smaller than found experimentally.

For an approximately constant chiral angle, but varying diameter, the intensity ratios calculated for two tubes agree quite well with experiment. Constant chiral angle, but varying diameter means comparing two tubes from different branches with constant $n-m$. For example, the (10,2) is slightly more intense than the (9,1); the (8,4) is stronger than the (7,3) [other pairs in Fig. 4 that almost match the criterion are (9,2) vs (8,1), (7,6) vs (6,5), and (9,4) vs (8,3); their experimental intensity ratio in Fig. 4(a) is well-described by the tight-binding calculations, Fig. 4(b)]. On the other hand, for approximately constant diameter but varying chiral angle ($2n+m=$const, see dashed lines in Fig. 4) the experimental data deviate quite strongly from the predictions [(6,5) vs (8,1), (8,3) vs (9,1) etc.]. There is a discrepancy in the genuine dependence on chiral angle between the experimental and calculated intensities.

Assuming the differences between theory and experiment in Fig. 4 to be due to the (n,m) abundance of the tubes, we find a ratio of $\approx$3 between large (close-to armchair) and small chiral angles (zigzag). This difference is much smaller than deduced from PLE for this type of sample.[6] For a homogeneous chiral angle distribution, on the other hand, the combined optical and electron-phonon matrix element is overestimated in zigzag tubes. Since nanotube excitations are excitons,[25,26] whereas the calculations assumed uncorrelated electron-hole pairs, an overall factor of 3 for the intensities (or 1.7 for the product of the squared optical times the electron-phonon matrix element) is a quite reasonable agreement. Further experimental and theoretical studies are under way to clarify this point.

In conclusion, we showed that the Raman intensity depends sensitively on electron subbands (E_{11} vs E_{22}), the nanotube family, and the chiral angle. To use Raman intensities for the investigation of abundances of different chiral indices, these dependences need to be fully included. The E_{11}^S transition is better suited for such an endeavor because of the absence of exciton-exciton resonances, in contrast to the E_{22}^S transitions. We found that the intensity difference between nanotube families $\nu=\pm1$ is much smaller and reversed for E_{11}^S transitions compared to excitations into E_{22}^S. For our particular sample we find an approximately homogeneous distribution of chiral angles in the range $6.7\leqslant d\leqslant 9$ Å.

We thank T. Warming and E. Stock for providing the equipment and for much appreciated support with the experiments. The samples were kindly provided by F. Hennrich.

*Electronic address: telg@physik.tu-berlin.de

[1] S. Reich, C. Thomsen, and J. Maultzsch, *Carbon Nanotubes: Basic Concepts and Physical Properties* (Wiley-VCH, Berlin, 2004).
[2] B. Kitiyanan, W. E. Alvarez, J. H. Harwell, and D. E. Resasco, Chem. Phys. Lett. **317**, 497 (2000).
[3] S. Reich, L. Li, and J. Robertson, Chem. Phys. Lett. **421**, 469 (2006).
[4] M. Zheng, A. Jagota, M. S. Strano, A. P. Santos, P. Barone, S. G. Chou, B. A. Diner, M. S. Dresselhaus, R. S. McLean, G. B. Onoa, G. G. Samsonidze, E. D. Semke, M. Usrey, and D. J. Walls, Science **302**, 1545 (2003).
[5] R. Krupke, F. Hennrich, H. v. Löhneysen, and M. M. Kappes, Science **301**, 344 (2003).
[6] S. M. Bachilo, M. S. Strano, C. Kittrell, R. H. Hauge, R. E. Smalley, and R. B. Weisman, Science **298**, 2361 (2002).
[7] H. Telg, J. Maultzsch, S. Reich, F. Hennrich, and C. Thomsen, Phys. Rev. Lett. **93**, 177401 (2004).
[8] C. Fantini, A. Jorio, M. Souza, M. S. Strano, M. S. Dresselhaus, and M. A. Pimenta, Phys. Rev. Lett. **93**, 147406 (2004).
[9] Y. Miyauchi, S. Chiashi, Y. Murakami, Y. Hayashida, and S. Maruyama, Chem. Phys. Lett. **387**, 198 (2004).
[10] A. Jorio, A. P. Santos, H. B. Ribeiro, C. Fantini, M. Souza, J. P. M. Vieira, C. A. Furtado, J. Jiang, R. Saito, L. Balzano, D. E. Resasco, and M. A. Pimenta, Phys. Rev. B **72**, 075207 (2005).
[11] S. Reich and C. Thomsen, Phys. Rev. B **62**, 4273 (2000).
[12] M. Machón, S. Reich, H. Telg, J. Maultzsch, P. Ordejón, and C. Thomsen, Phys. Rev. B **71**, 035416 (2005).
[13] V. N. Popov, L. Henrard, and Ph. Lambin, Nano Lett. **4**, 1795 (2004).
[14] S. Reich, C. Thomsen, and J. Robertson, Phys. Rev. Lett. **95**, 077402 (2005).
[15] C. L. Kane and E. J. Mele, Phys. Rev. Lett. **90**, 207401 (2003).
[16] S. Lebedkin, F. Hennrich, T. Skipa, and M. M. Kappes, J. Phys. Chem. B **107**, 1949 (2003).
[17] M. J. O'Connell, S. M. Bachilo, C. B. Huffman, V. C. Moore, M. S. Strano, E. H. Haroz, K. L. Rialon, P. J. Boul, W. H. Noon, C. Kittrell, J. P. Ma, R. H. Hauge, R. B. Weisman, and R. E. Smalley, Science **297**, 593 (2002).
[18] M. Cardona, in *Light Scattering in Solids II*, edited by M. Cardona and G. Güntherodt, Vol. 50 of *Topics in Applied Physics* (Springer, Berlin, 1982), p. 19.
[19] C. Thomsen and S. Reich, in *Light Scattering in Solids IX*, edited by M. Cardona and R. Merlin, *Topics in Applied Physics* (Springer, Berlin, 2006) (in print).
[20] S. Reich, J. Maultzsch, C. Thomsen, and P. Ordejón, Phys. Rev. B **66**, 035412 (2002).
[21] J. Maultzsch, H. Telg, S. Reich, and C. Thomsen, Phys. Rev. B **72**, 205438 (2005).
[22] R. B. Weisman and S. M. Bachilo, Nano Lett. **3**, 1235 (2003).
[23] S. K. Doorn, D. A. Heller, P. W. Barone, M. L. Usrey, and M. S. Strano, Appl. Phys. A: Mater. Sci. Process. **78**, 1147 (2004).
[24] S. V. Goupalov, B. C. Satishkumar, and S. K. Doorn, Phys. Rev. B **73**, 115401 (2006).
[25] F. Wang, G. Dukovic, L. E. Brus, and T. Heinz, Science **308**, 838 (2005).
[26] J. Maultzsch, R. Pomraenke, S. Reich, E. Chang, D. Prezzi, A. Ruini, E. Molinari, M. S. Strano, C. Thomsen, and C. Lienau, Phys. Rev. B **72**, 241402(R) (2005).